

# A 2-D Organic-Inorganic Hybrid [Cu(En)<sub>2</sub>(H<sub>2</sub>O)]<sub>2</sub>[Cu(En)<sub>2</sub>]<sub>4</sub>[Si<sub>2</sub>Cu<sub>2</sub>W<sub>22</sub>O<sub>78</sub>] · 7H<sub>2</sub>O Assembled from Monocopper(II)-Substituted Keggin Silicotungstate Dimers<sup>1</sup>

J. Luo<sup>a, b</sup>, L. J. Chen<sup>a, b, \*</sup>, D. Y. Shi<sup>a</sup>, Y. Y. Li<sup>a</sup>, and J. W. Zhao<sup>a</sup>

<sup>a</sup> Institute of Molecular and Crystal Engineering, College of Chemistry and Chemical Engineering, Henan University, Kaifeng, Henan 475004, P.R. China

<sup>b</sup> Basic Experiment Teaching Center, Henan University, Kaifeng, Henan 475004, P.R. China

\*e-mail: ljchen@henu.edu.cn, zhaojunwei@henu.edu.cn

Received August 10, 2011

**Abstract**—The reaction of Na<sub>10</sub>[A-α-SiW<sub>9</sub>O<sub>34</sub>] · 18H<sub>2</sub>O with CuCl<sub>2</sub> · 2H<sub>2</sub>O in the participation of ethylenediamine (En) under hydrothermal conditions resulted in a 2D organic-inorganic hybrid monocopper(II)-substituted Keggin silicotungstate [Cu(En)<sub>2</sub>(H<sub>2</sub>O)]<sub>2</sub>[Cu(En)<sub>2</sub>]<sub>4</sub>[Si<sub>2</sub>Cu<sub>2</sub>W<sub>22</sub>O<sub>78</sub>] · 7H<sub>2</sub>O (**I**), which was structurally characterized by elemental analyses, IR spectrum, UV spectrum, powder X-ray diffraction (PXRD), and single-crystal X-ray diffraction. Single crystal structural analysis shows that adjacent monocopper(II)-substituted Keggin silicotungstate [Si<sub>2</sub>Cu<sub>2</sub>W<sub>22</sub>O<sub>78</sub>]<sup>12-</sup> dimeric subunits are interconnected by sharing terminal oxygen atoms to make the 1D polymeric linear chain and neighboring chains are combined with each other through [Cu(En)<sub>2</sub>]<sup>2+</sup> connectors giving rise to an interesting 2D organic-inorganic hybrid sheet architecture with a 4-connected topology. To our knowledge, **I** is the rare organic-inorganic hybrid 2D polyoxometate constructed by mono-transition-metal substituted Keggin silicotungstate dimeric subunits. The photocatalytic measurement illustrates that **I** can to some extent inhibit the photodegradation of rhodamine-B.

**DOI:** 10.1134/S1070328412120032

## INTRODUCTION

Polyoxometalates (POMs), as a unique class of fascinating metal-oxygen cluster species with enormous structural varieties and interesting properties, have been extensively studied due to their actual and potential applications in diverse fields, such as catalysis, material science and magnetism [1–4]. It has been long recognized that the incorporation of transition-metal complexes (TMCs) to the lacunary POM matrixes or surfaces provides a very effective approach for the design and preparation of novel inorganic-organic hybrid POM-based materials that bear both features of inorganic and organic components [5]. The *in-situ* formed TMCs can function as charge compensation cations, modify inorganic POM surfaces and frameworks, or join discrete clusters into extended architectures [6]. Recently, we have concentrated on the exploration on the hydrothermal reactivity of lacunary POM precursors with electrophilic transition-metal (TM) cations in the participation of organic ligands with aim of discovering novel TMCs-containing POMs with unexpected structures and properties. Thus, a family of unique TMCs-containing POMs have been prepared in our lab, such as a CdSO<sub>4</sub>-like 3D framework [Cu(En)<sub>2</sub>]<sub>3</sub>[α-AsW<sub>11</sub>NaO<sub>39</sub>] · 2H<sub>2</sub>O [7], three multi-nickel substituted arsenotungstates

[EnH<sub>2</sub>]<sub>2</sub>[Ni(H<sub>2</sub>O)<sub>4</sub>]<sub>2</sub>[Ni(En)<sub>2</sub>]<sub>2</sub>[Ni(En)]<sub>2</sub>{[(α-AsW<sub>6</sub>O<sub>26</sub>)Ni<sub>6</sub>(OH)<sub>2</sub>(H<sub>2</sub>O)<sub>3</sub>(En)(B-α-AsW<sub>6</sub>O<sub>34</sub>)<sub>2</sub>][W<sub>4</sub>O<sub>16</sub>][Ni<sub>3</sub>(H<sub>2</sub>O)<sub>2</sub>(En)]<sub>2</sub>} · 16H<sub>2</sub>O [8], [Ni(H<sub>2</sub>O)(En)<sub>2</sub>]<sub>2</sub>[Ni(H<sub>2</sub>O)<sub>3</sub>(En)][Ni(H<sub>2</sub>O)(En)]{[(α-AsW<sub>6</sub>O<sub>26</sub>)Ni<sub>6</sub>(OH)<sub>2</sub>(En)<sub>2.5</sub>(B-α-AsW<sub>6</sub>O<sub>34</sub>)<sub>2</sub>H<sub>4</sub>][W<sub>4</sub>O<sub>16</sub>][Ni<sub>4</sub>(H<sub>2</sub>O)<sub>2</sub>(En)<sub>2</sub>]} · 13H<sub>2</sub>O [8], and [Na(H<sub>2</sub>O)<sub>3</sub>]<sub>2</sub>[Ni(H<sub>2</sub>O)<sub>6</sub>]<sub>2</sub>[Ni(H<sub>2</sub>O)<sub>5</sub>]{[Ni<sub>3</sub>(Dap)(H<sub>2</sub>O)<sub>2</sub>]<sub>2</sub>(H<sub>2</sub>W<sub>4</sub>O<sub>16</sub>)}{(α-H<sub>2</sub>AsW<sub>6</sub>O<sub>26</sub>)Ni<sub>6</sub>(OH)<sub>2</sub>(H<sub>2</sub>O)(Dap)<sub>2</sub>}(B-α-HAsW<sub>6</sub>O<sub>34</sub>)<sub>2</sub>} · 7H<sub>2</sub>O (Dap = 1,2-diaminopropane) [9] and a dimer [EnH<sub>2</sub>]<sub>4</sub>{[Cu(En)<sub>2</sub>][(A-β-H<sub>2</sub>AsW<sub>9</sub>O<sub>34</sub>)Cu(En)<sub>2</sub>]} · 8H<sub>2</sub>O containing [A-β-AsW<sub>9</sub>O<sub>34</sub>]<sup>9-</sup> fragments [10]. As a part of our ongoing work, the hydrothermal reaction of Na<sub>10</sub>[A-α-SiW<sub>9</sub>O<sub>34</sub>] · 18H<sub>2</sub>O with CuCl<sub>2</sub> · 2H<sub>2</sub>O in the presence of En led to a 2D organic-inorganic hybrid monocopper(II)-substituted Keggin silicotungstate [Cu(En)<sub>2</sub>(H<sub>2</sub>O)]<sub>2</sub>[Cu(En)<sub>2</sub>]<sub>4</sub>[Si<sub>2</sub>Cu<sub>2</sub>W<sub>22</sub>O<sub>78</sub>] · 7H<sub>2</sub>O (**I**). Interestingly, adjacent monocopper(II)-substituted [Si<sub>2</sub>Cu<sub>2</sub>W<sub>22</sub>O<sub>78</sub>]<sup>12-</sup> dimeric subunits are interconnected by sharing terminal oxygen atoms to make the 1D polymeric linear chain and neighboring chains are combined with each other through [Cu(En)<sub>2</sub>]<sup>2+</sup> connectors giving rise to an interesting 2D organic-inorganic hybrid sheet architecture with a 4-connected topology. Although several 0D and 1D monocopper(II)-substituted Keggin silicotungstates, such as K<sub>5</sub>[Cu(Ac)(Pmdien)][SiW<sub>11</sub>CuO<sub>39</sub>] · 12H<sub>2</sub>O (Ac = acetate, Pmdien = N,N,N',N'',N''-pentamethyldi-

<sup>1</sup> The article is published in the original.

ethylentriamine) [11],  $K_{14}[\{Cu_2(Bipy)_2(\mu-Ox)\}\{SiW_{11}O_{39}Cu(H_2O)\}]_2[SiW_{11}O_{39}Cu(H_2O)] \cdot \sim 55H_2O$  (Bipy = 2,2'-bipyridine, Ox = oxalate) [12],  $K_4[\{SiW_{11}O_{39}Cu(H_2O)\}\{Cu_2(Ac)_2(Phen)_2(H_2O)\}] \cdot 14H_2O$  (Phen = phenanthroline) [13], and  $\{[Cu(Deta)(H_2O)_2]_2[Cu(Deta)(H_2O)][\alpha-XCuW_{11}O_{39}]\} \cdot 5H_2O$  (Deta = diethylenetriamine) [5] have been reported. To our knowledge, **I** is a rare organic-inorganic hybrid 2D POM constructed by mono-TM substituted Keggin silicotungstate dimeric subunits. By means of UV-visible spectra, we examined the degradation of the rhodamine-B by the 500 W Hg lamp irradiation in the presence of **I** as the photocatalyst.

## EXPERIMENTAL

**Materials and methods.**  $Na_{10}[A-\alpha-SiW_9O_{34}] \cdot 18H_2O$  was prepared according to the literature [14] and confirmed by IR spectrum. All other chemicals used for synthesis were reagent grade and used without further purification. Elemental analyses (C, H, and N) were performed on a Perkin-Elmer 240C elemental analyzer. The IR spectrum was recorded from a sample powder palletized with KBr on a Nicolet FT-IR 360 spectrometer in the range of 4000–400  $cm^{-1}$ . The UV-visible spectrum was obtained with a U-4100 spectrometer at room temperature. PXRD measurement was performed on a Philips X'Pert-MPD instrument with  $CuK_{\alpha}$  radiation ( $\lambda = 1.54056 \text{ \AA}$ ) in the angular range  $2\theta = 10^\circ - 45^\circ$  at 293 K.

**Synthesis of I.**  $Na_{10}[A-\alpha-SiW_9O_{34}] \cdot 18H_2O$  (0.300 g, 10.788 mmol) and  $Cu(CH_3COO)_2 \cdot H_2O$  (0.063 g, 31.555 mmol) were suspended in  $H_2O$  (5 mL), to which En (0.050 mL, 0.740 mmol) was added under stirring. The resulting mixture was stirred for 3 h, sealed in a 25 mL Teflon-lined stainless steel autoclave, kept for 5 days at  $160^\circ C$  and then cooled to room temperature. Purple prismatic crystals were filtered, washed with distilled water and dried in air at ambient temperature. The yield was ~41% (based on  $Na_{10}[A-\alpha-SiW_9O_{34}] \cdot 18H_2O$ ).

For  $C_{24}H_{114}N_{24}O_{87}Si_2Cu_8W_{22}$

anal. calcd., %: C, 4.28; H, 1.70; N, 4.99.

Found, %: C, 4.35; H, 1.86; N, 4.90.

As **I** contains the monovacant Keggin  $[\alpha-SiW_{11}O_{39}]^{8-}$  fragments, when the precursor  $[\alpha-SiW_{11}O_{39}]^{8-}$  in place of  $[A-\alpha-SiW_9O_{34}]^{10-}$  was used to react with  $Cu(CH_3COO)_2 \cdot H_2O$  under similar conditions, we failed to obtain **I**. The result indicates that  $[A-\alpha-SiW_9O_{34}]^{10-}$  plays an important role in the formation of **I**. Interestingly, the transformation of the trivacant  $[A-\alpha-SiW_9O_{34}]^{9-}$  to the monovacant  $[\alpha-SiW_{11}O_{39}]^{8-}$  occurred, which is very similar to the evolution of  $[A-\alpha-PW_9O_{34}]^{9-} \rightarrow [\alpha-PW_{11}O_{39}]^{7-}$  in

the preparation of the  $3d-4f$  heterometallic POM  $[Cu(Dap)_2(H_2O)][Cu(Dap)_2]_{4,5}[Gd(\alpha-PW_{11}O_{39})_2] \cdot 5H_2O$  reported by us [15].

**X-ray crystal determination.** A purple prismatic crystal was carefully selected under an optical microscope and glued at the tip of a thin glass fiber with cyanoacrylate adhesive. Intensity data were collected on a Bruker APEX-II CCD detector at 296(2) K with a  $MoK_{\alpha}$  radiation ( $\lambda = 0.71073 \text{ \AA}$ ). Direct methods were used to solve the structures and to locate the heavy atoms using the SHELXTL-97 program package [16]. The remaining atoms were found from successive full-matrix least-squares refinements on  $F^2$  and Fourier syntheses. Lorentz polarization and empirical absorption corrections were applied. In **I**, the W(3), W(12), W(13), and W(22) positions are simultaneously statistically occupied by copper(II) and tungsten(VI) elements with half occupancy for each, resulting in one expected  $Cu^{2+}$  ion per Keggin cage on the charge balance and crystallographic considerations, which is very common in POM chemistry [5, 17]. All of the non-hydrogen atoms were refined anisotropically. All hydrogen atoms were placed in the idealized positions and refined with a riding model using default SHELXL parameters. The hydrogen atoms attached to lattice water molecules were not located. The weighting detail:  $w = 1/[\sigma^2(F_o^2) + (0.0599P)^2 + 448.2024P]$ , where  $P = (F_o^2 + 2F_c^2)/3$ . The crystallographic data are listed in table. The atomic coordinates and other parameters of structure **I** have been deposited with the Cambridge Crystallographic Data Centre (no. 838105; deposit@ccdc.cam.ac.uk or <http://www.ccdc.cam.ac.uk>).

## RESULTS AND DISCUSSION

In order to characterize the purity of **I**, the PXRD has been measured. The experimental PXRD pattern of the bulk product of **I** is in good consistent with the simulated PXRD pattern from single-crystal X-ray diffraction, showing that the phase of the sample is pure (Fig. 1). Both differences in intensity are related to the variation in preferred orientation of the powder sample during collection of the experimental PXRD. X-ray single-crystal structure analysis indicates that the molecular structural unit of **I** (Fig. 2a) consists of a monocopper(II)-substituted Keggin silicotungstate  $[Si_2Cu_2W_{22}O_{78}]^{12-}$  dimeric subunit, one discrete  $[Cu(En)_2(H_2O)]^{2+}$  cation, three supporting  $[Cu(En)_2]^{2+}$  cations, one supporting  $[Cu(En)_2(H_2O)]^{2+}$  cation and one bridging  $[Cu(En)_2]^{2+}$  cation and seven lattice water molecules. Notably, there are six crystallographically unique  $Cu^{2+}$  cations (Cu(1), Cu(2), Cu(3), Cu(4), Cu(5), and Cu(6)) in **I**. The supporting  $[Cu(1)(En)_2]^{2+}$ ,  $[Cu(3)(En)_2]^{2+}$ , and  $[Cu(6)(En)_2]^{2+}$  cations inhabit in the square pyramid geometry estab-

Crystallographic data and structural refinements for **I**

Parameter	Value
Formula weight	6740.45
Crystal system	Monoclinic
Space group	$P2_1/c$
$a$ , Å	18.811(2)
$b$ , Å	23.063(3)
$c$ , Å	26.039(4)
$\beta$ , deg	96.267(3)
$V$ , Å <sup>3</sup>	11 230(3)
$Z$	4
$\rho_{\text{calcd}}$ , g cm <sup>-3</sup>	3.987
$\mu$ , mm <sup>-1</sup>	24.040
$F(000)$	12034
Crystal size, mm	0.44 × 0.32 × 0.27
Limiting indices	$-21 \leq h \leq 22, -22 \leq k \leq 27, -27 \leq l \leq 30$
$\theta$ Range for data collection, deg	1.55–25.00
Type of scan	$\varphi$ and $\omega$ scan
Reflections collected/unique ( $R_{\text{int}}$ )	55948/19637 (0.1031)
Number of reflections, $I > 2\sigma(I)$	13766
Number of parameters refined	1249
Goodness-of-fit on $F^2$	1.043
Final $R$ indices ( $I > 2\sigma(I)$ )	$R_1 = 0.0775, wR_2 = 0.1674$
$R$ indices (all data)	$R_1 = 0.1105, wR_2 = 0.1809$
$\Delta\rho_{\text{max}}/\Delta\rho_{\text{min}}$ , e Å <sup>-3</sup>	5.262/−4.417

lished by four nitrogen atoms from two En ligands (Cu–N 1.95(2)–2.07(2) Å) and one terminal oxygen atom from the  $[\text{Si}_2\text{Cu}_2\text{W}_{22}\text{O}_{78}]^{12-}$  dimeric subunit (Cu–O 2.30(2)–2.53(2) Å). The supporting

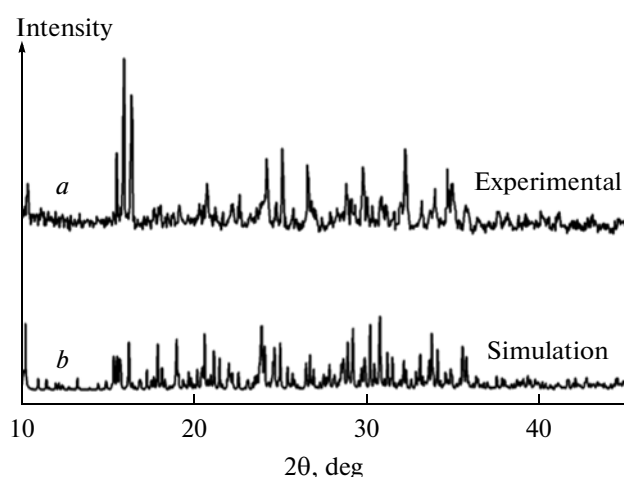


**Fig. 1.** The PXRD pattern of **I** (a) and its calculated pattern (b) based on the single-crystal solution.

$[\text{Cu}_2(\text{En})_2(\text{H}_2\text{O})]^{2+}$  cation adopts the six-coordinate octahedral geometry, in which four nitrogen atoms from two En ligands build the basal plane (Cu–N 1.99(3)–2.05(3) Å) and a terminal oxygen atom from the  $[\text{Si}_2\text{Cu}_2\text{W}_{22}\text{O}_{78}]^{12-}$  dimeric subunit (Cu–O 3.098(19) Å), and a water ligand (Cu–O 2.34(2) Å) stand on two axial positions. The bridging  $[\text{Cu}_4(\text{En})_2]^{2+}$  cation also utilizes the octahedral configuration, where four nitrogen atoms from two En ligands constitute the equatorial plane (Cu–N 1.94(3)–2.03(3) Å) and two terminal oxygen atoms from two neighboring  $[\text{Si}_2\text{Cu}_2\text{W}_{22}\text{O}_{78}]^{12-}$  dimeric subunits (Cu–O 2.478(19)–2.846(18) Å) occupy two axial sites. In addition, the discrete  $[\text{Cu}_5(\text{En})_2(\text{H}_2\text{O})]^{2+}$  cation is five-coordinate and exhibits a distorted square pyramidal geometry, in which the equatorial plane is defined by four nitrogen atoms from En ligands with Cu–N distances of 1.95(3)–2.00(3) Å, whereas the apical position is occupied by a water molecule with the Cu–O distance of 2.25(3) Å. The  $[\text{Si}_2\text{Cu}_2\text{W}_{22}\text{O}_{78}]^{12-}$  dimeric subunit can be viewed as a fusion of two monocopper substituted  $[\alpha\text{-SiCuW}_{11}\text{O}_{39}]^{6-}$  moieties through sharing a common oxygen atom. It should be noted that the W(3), W(12), W(13), and W(22) sites in **I** are simultaneously occupied by the Cu(II) and W(VI) atoms with half occupancy for each in two opposite  $\text{W}_3\text{O}_{13}$  trimers of each  $[\alpha\text{-SiCuW}_{11}\text{O}_{39}]^{6-}$  moiety. This disordered phenomenon has been observed in the previous study [5, 17].

Interestingly, adjacent  $[\text{Si}_2\text{Cu}_2\text{W}_{22}\text{O}_{78}]^{12-}$  dimeric subunits are interconnected together by sharing terminal oxygen atoms *via* Cu/W–O–Cu/W linkers, giving rise to the 1D infinite linear polymeric chain (Fig. 2b). This polymeric chain is very similar to those of  $[\text{ET}]_8[\text{PMnW}_{11}\text{O}_{39}] \cdot 2\text{H}_2\text{O}$  [18] (ET = *bis*(ethylenedithio)tetrathiofulvalene),  $[\text{NEt}_3\text{H}]_5[\text{XCoW}_{11}\text{O}_{39}] \cdot 3\text{H}_2\text{O}$  (X = P<sup>V</sup>/As<sup>V</sup>) [19] and  $\text{K}_3[\text{Cu}^{\text{I}}(4,4'\text{-Bi-py})_3[\text{SiCu}^{\text{II}}\text{W}_{11}\text{O}_{39}] \cdot 11\text{H}_2\text{O}$  [20], where Mn<sup>2+</sup>, Co<sup>2+</sup>, and Cu<sup>2+</sup> ions are disordered and  $[\text{Co}(\text{Dpa})_2(\text{OH}_2)_2]_2[\text{HDpa}][\text{PCoW}_{11}\text{O}_{39}]$  (Dpa = di-2-pyridylamine) [21], where the Co<sup>2+</sup> ion in the POM core is perfectly localized. More intriguingly, neighboring 1D linear polymeric chains are interconnected through  $[\text{Cu}_4(\text{En})_2]^{2+}$  connectors, generating an interesting 2D extended sheet architecture (Fig. 3a), as far as we know, which represents the rare organic-inorganic hybrid 2D POM constructed by mono-TM substituted Keggin silicotungstate dimeric subunits. In the 2D extended sheet, each the molecular structural unit of **I** is connected with four same units through sharing two terminal oxygen atoms and two  $[\text{Cu}_4(\text{En})_2]^{2+}$  connectors. From the viewpoint of topology, each the molecular structural unit of **I** can be viewed as a 4-connected node, the 2D extended sheet of **I** is a 4-connected topology network (Fig. 3b). Adjacent 2D 4-topological sheets are aligned in the mode of –ABAB– (Fig. 3b),

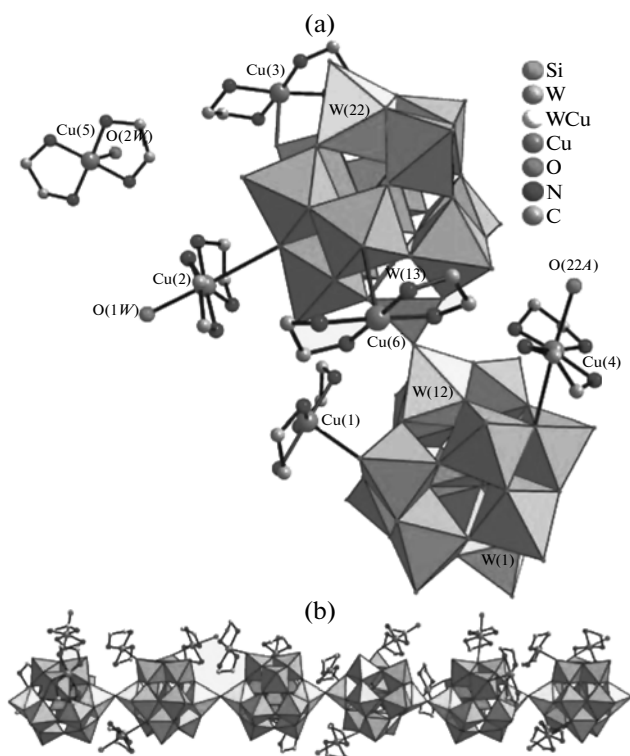


**Fig. 2.** The molecular structural unit of **I** with the selected labeling scheme (the atom with the suffix *A* is generated by the symmetry operation (*A*):  $x, 0.5 - y, 0.5 + z$ ) (a); the 1D infinite linear polymeric chain (b).

which is distinct from those reported POM-based 2D 4-topological sheets with the mode of  $-AAA-$  [22, 23].

The comparison of the IR spectra of **I** and  $\text{Na}_{10}[A-\alpha\text{-SiW}_9\text{O}_{34}] \cdot 18\text{H}_2\text{O}$  is shown in Fig. 4. The IR spectrum of **I** displays the characteristic vibration patterns derived from the Keggin-type polyoxoanion in the range of  $1100\text{--}600\text{ cm}^{-1}$ . The characteristic vibration bands at  $998, 947, 894$  and  $790, 686\text{ cm}^{-1}$  are attributed to  $\nu(\text{W}-\text{O}_t)$ ,  $\nu(\text{Si}-\text{O}_a)$ ,  $\nu(\text{W}-\text{O}_b)$ , and  $\nu(\text{W}-\text{O}_c)$ , respectively [24]. In general, these characteristic bands can be easily assigned by comparing with the corresponding bands of monovacant or plenary Keggin clusters. The  $\nu(\text{W}-\text{O}_c)$  mode, observed as a single signal for plenary Keggin cluster  $[\alpha\text{-SiW}_{12}\text{O}_{40}]^{4-}$ , splits into two bands in the spectra of **I**, the main reason of which is related to the lower symmetry of the  $[\alpha\text{-SiW}_{11}\text{O}_{39}]^{8-}$  moieties in **I** in contrast to the  $[\alpha\text{-SiW}_{12}\text{O}_{40}]^{4-}$  cluster. Obviously, the IR spectra of **I** and  $\text{Na}_{10}[A-\alpha\text{-SiW}_9\text{O}_{34}] \cdot 18\text{H}_2\text{O}$  are somewhat different, which further confirms the structural transformation of the trivacant  $[A-\alpha\text{-SiW}_9\text{O}_{34}]^{9-}$  moiety in the starting material to the monovacant  $[\alpha\text{-SiW}_{11}\text{O}_{39}]^{8-}$  moiety in **I**. Compared with the IR spectrum of  $\alpha\text{-K}_8\text{SiW}_{11}\text{O}_{39} \cdot 13\text{H}_2\text{O}$  [25], the  $\nu(\text{W}-\text{O}_t)$  vibration peak for **I** has a red-shift of  $13\text{ cm}^{-1}$ , the possible reason for

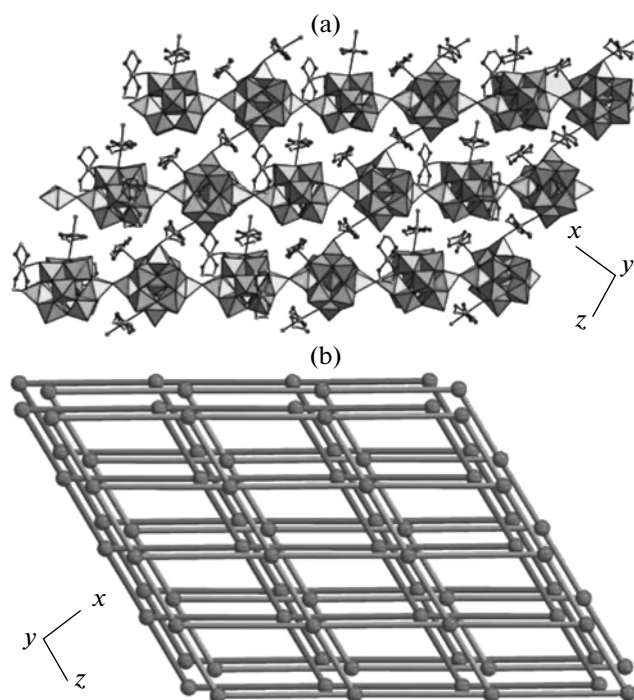


**Fig. 3.** The 2D extended sheet architecture (a); the 2D 4-connected topology showing the alignment mode of  $-ABAB-$  (b).

which is related to the stronger interactions between  $[\text{Cu}(\text{En})_2]^{2+}/[\text{Cu}(\text{En})_2(\text{H}_2\text{O})]^{2+}$  cations and terminal oxygen atoms of the  $[\text{Si}_2\text{Cu}_2\text{W}_{22}\text{O}_{78}]^{12-}$  dimeric sub-units. In addition, the resonances at  $3299\text{--}3247$  and

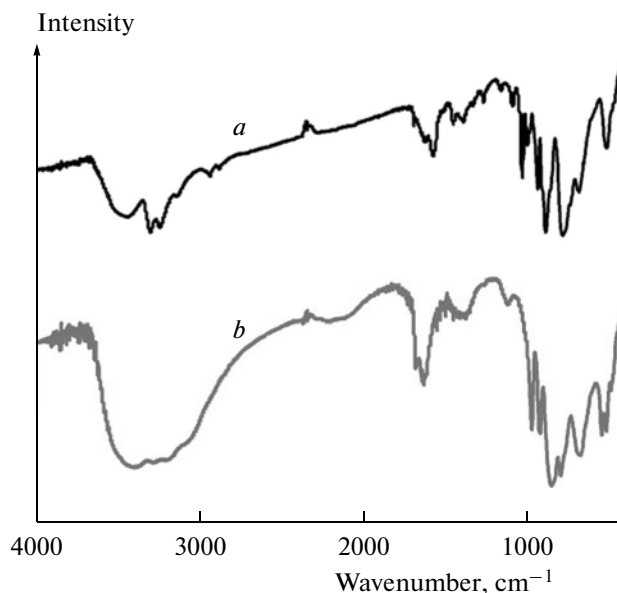


**Fig. 4.** Comparison of the IR spectra of **I** (a) and  $\text{Na}_{10}[A-\alpha\text{-SiW}_9\text{O}_{34}] \cdot 18\text{H}_2\text{O}$  (b).

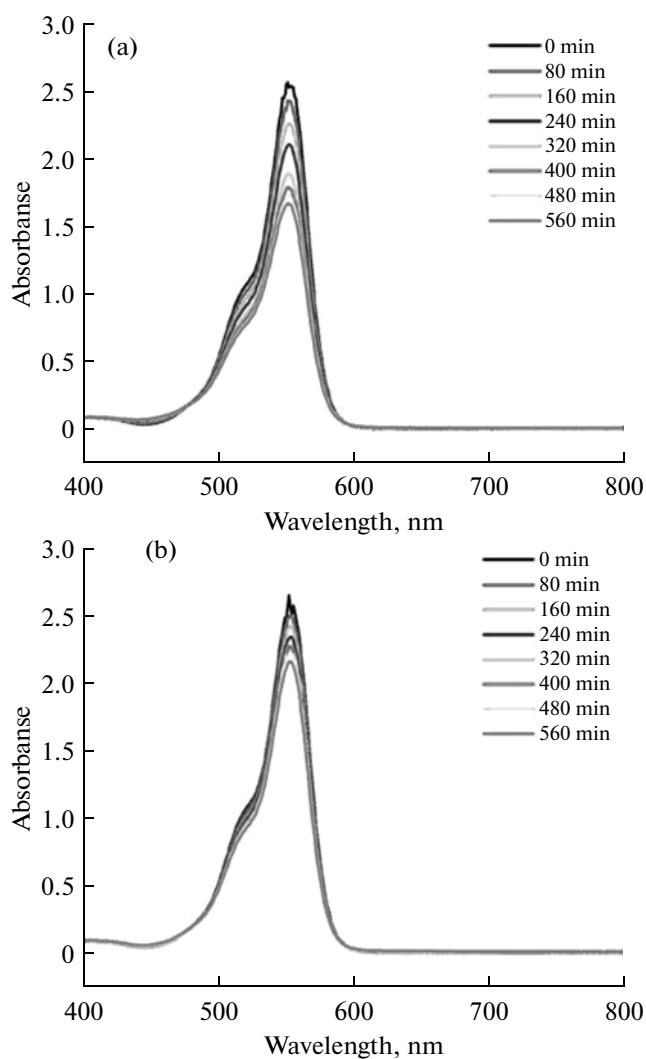


**Fig. 5.** UV-visible absorption spectral changes observed for the rhodamine-B solutions at various irradiation times in the absence of **I** (a) and in the presence of **I** (b).

2942–2882  $\text{cm}^{-1}$  are assigned to the  $\nu(\text{NH}_2)$  and  $\nu(\text{CH}_2)$  stretching vibrations, and the signals at 1587 and 1460  $\text{cm}^{-1}$  respond to the  $\delta(\text{NH}_2)$  and  $\delta(\text{CH}_2)$  bending vibrations, respectively. These resonance signals illustrate the presence of En ligands in **I** [8]. The occurrence of the vibration band at 3455  $\text{cm}^{-1}$  suggests the presence of the lattice water molecules or coordination water molecules in **I**. In short, the result of the IR spectrum is in good agreement with the single-crystal structural analysis. The UV spectrum of **I** has been performed in aqueous solution in the range of 190–400 nm at room temperature. The UV spectrum of **I** reveals two characteristic absorption bands, appearing at 195 and 250 nm. The higher energy band can be assigned to  $\text{O}_t \rightarrow \text{W}$  charge transfer absorption band, whereas the lower energy band is attributed to

$\text{O}_{b(c)} \rightarrow \text{W}$  charge transitions, which is characteristic of Keggin-type cluster.

In order to investigate the photocatalytic property of **I**, the photocatalytic degradation of rhodamine-B by the 500 W Hg lamp irradiation has been performed when **I** acts as a photocatalyst. The typical photocatalytic reaction process is as follows:  $3.0 \times 10^{-3}$  mmol of **I** was added to a 25 mL of solution of rhodamine-B ( $3.0 \times 10^{-5}$  mol  $\text{L}^{-1}$ ) and then magnetically stirred in the dark for about 5 min. The suspension solution was then exposed to the 500 W Hg lamp irradiation under stirring for 560 min. Every 80 min, the same amount of solution was taken out to carry out the UV-visible spectral detection. As we know, the rhodamine-B substrate containing four N-ethyl groups at either side of the xanthen ring is relatively stable in aqueous solution in darkness or upon visible light irradiation [26, 27]. When the rhodamine-B substrate is kept in darkness either in the presence of **I** or in the absence of **I**, the degradation reaction of rhodamine-B substrate hardly occurs. Upon UV irradiation, the rhodamine-B substrate in the absence of **I** exhibits a comparatively obvious photodegradation phenomenon in aqueous solution and the UV-visible spectral maximum absorbance of the degradation solution decreases from 2.53 to 1.64 after 560 min (Fig. 5a). The UV-visible spectral evolution on the photodegradation of rhodamine-B at various times in the presence of **I** is shown in Fig. 5b. In comparison with that in the absence of **I**, obviously, the UV-visible spectral maximum absorbance of the degradation solution in the presence of **I** slowly decreases from 2.53 to 2.15 after 560 min, which suggests that **I** can to some degree inhibit the photodegradation of rhodamine-B, which is completely distinct from those that can accelerate the photodegradation of rhodamine-B [28, 29]. The main reasons that **I** can inhibit the photodegradation of rhodamine-B may be as follows: (a) **I** can function as an absorber of the Hg lamp irradiation; (b) the hydrogen-bonding interactions between donors and acceptors in rhodamine-B substrates ( $\text{N}(\text{C}_2\text{H}_5)_2$ ,  $\text{COOH}$ ) and **I** (En and surface oxygen atoms of POMs) enhance the chemical stability of rhodamine-B substrates in the solutions, which leads to the slow photodegradation of rhodamine-B substrates. Currently, the profound study on the mechanism of photocatalysis of rhodamine-B in the presence of **I** as the photocatalyst is underway.

#### ACKNOWLEDGMENTS

We are thankful for financial support from the Natural Science Foundation of China (nos. 21071043, 21071042), the China Postdoctoral Science Foundation funded project (no. 20100470996), the Natural Science Foundation of Henan Province (nos. 092300410119, 102300410093), the Natural Science Foundation of Henan University (no. 2008YBZR010), the Postdoc-

toral Science Foundation of Henan University (no. BH2010003), the Foundation of Education Department of Henan Province (nos. 2009A150003, 2010B150006), and the Students Innovative Pilot Plan of Henan University (no. 09NB005).

## REFERENCES

1. Compain, J.D., Mialane, P., Dolbecq, A., et al., *Angew. Chem. Int. Ed.*, 2009, vol. 48, p. 3077.
2. Zhang, Z.M., Yao, S., Li, Y.G., et al., *Chem. Commun.*, 2008, p. 1650.
3. Guo, D.J., Fu, S.J., Tan, W., et al., *J. Mater. Chem.*, 2010, vol. 20, p. 10159.
4. Liu, C.M., Zhang, D.Q., and Zhu, D.B., *Chem. Asian J.*, 2011, vol. 6, p. 74.
5. Zhao, J.W., Zhang, S.T., and Yang, G.Y., *J. Solid State Chem.*, 2008, vol. 181, p. 2205.
6. Reinoso, S., Vitoria, P., and Felices, L.S., *Inorg. Chem.*, 2007, vol. 46, p. 1237.
7. Zhao, J.W., Han, Q.X., Chen, L.J., et al., *Inorg. Chem. Commun.*, 2009, vol. 12, p. 707.
8. Zhao, J.W., Shi, D.Y., Chen, L.J., et al., *CrystEngComm.*, 2011, vol. 13, p. 3462.
9. Chen, L.J., Zhao, J.W., Ma, P.T., et al., *Inorg. Chem. Commun.*, 2010, vol. 13, p. 50.
10. Liu, Y., Shi, D.Y., and Zhao, J.W., *Inorg. Chem. Commun.*, 2011, vol. 14, p. 1178.
11. Felices, L.S., Vitoria, P., Gutiérrez-Zorrilla, J.M., et al., *Chem. Eur. J.*, 2004, vol. 10, p. 5138.
12. Reinoso, S., Vitoria, P., Lezama, L., et al., *Inorg. Chem.*, 2003, vol. 42, p. 3709.
13. Reinoso, S., Vitoria, P., Felices, L.S., et al., *Inorg. Chem.*, 2006, vol. 45, p. 108.
14. Hervé, G. and Tézé, A., *Inorg. Chem.*, 1977, vol. 16, p. 2115.
15. Liu, Y., Shi, D.Y., Zhao, J.W., et al., *Russ. J. Coord. Chem.*, 2011, vol. 37, p. 712.
16. Sheldrick, G.M., *SHELXTL-97, Program for Crystal Structure Solution*, Göttingen (Germany): Univ. of Göttingen, 1997.
17. Reinoso, S., Vitoria, P., Felices, L.S., et al., *Chem. Eur. J.*, 2005, vol. 11, p. 1538.
18. Galán-Mascarós, J.R., Giménez-Saiz, C., Triki, S., et al., *Angew. Chem. Int. Ed.*, 1995, vol. 34, p. 1460.
19. Evans, H.T., Weakley, T.J.R., and Jameson, G.B., *Dalton Trans.*, 1996, p. 2573.
20. Felices, L.S., Vitoria, P., and Gutiérrez-Zorrilla, J.M., *Inorg. Chem.*, 2006, vol. 45, p. 7748.
21. Yan, B.B., Xu, Y., Bu, X.H., et al., *Dalton Trans.*, 2001, p. 2009.
22. Zhao, J.W., Li, B., Zheng, S.T., et al., *Cryst. Growth Des.*, 2007, vol. 7, p. 2658.
23. Shi, D.Y., Chen, L.J., Zhao, J.W., et al., *Inorg. Chem. Commun.*, 2011, vol. 14, p. 324.
24. Wang, J.P., Zhao, J.W., Duan, X.Y., et al., *Cryst. Growth Des.*, 2006, vol. 6, p. 507.
25. Niu, J.Y., Zhao, J.W., and Wang, J.P., *J. Mol. Struct.*, 2004, vol. 701, p. 19.
26. Tao, X., Ma, W.H., Zhang, T.Y., et al., *Chem. Eur. J.*, 2002, vol. 8, p. 1321.
27. Chen, W.L., Chen, B.W., Tan, H.Q., et al., *J. Solid State Chem.*, 2010, vol. 183, p. 310.
28. Chen, C.C., Zhao, W., Lei, P.X., et al., *Chem. Eur. J.*, 2004, vol. 10, p. 1956.
29. Wu, Q., Chen, W.L., Liu, D., et al., *Dalton Trans.*, 2011, vol. 40, p. 56.

SPELL: 1. Spectrochim